

Invasive species detection in Hawaiian rainforests using airborne imaging spectroscopy and LiDAR

Gregory P. Asner^{a,*}, David E. Knapp^a, Ty Kennedy-Bowdoin^a, Matthew O. Jones^a,
Roberta E. Martin^a, Joseph Boardman^b, R. Flint Hughes^c

^a Department of Global Ecology, Carnegie Institution, 260 Panama Street, Stanford, CA 94305, USA

^b Analytical Imaging and Geophysics LLC, Boulder, CO 80302, USA

^c Institute of Pacific Islands Forestry, USDA Forest Service, Hilo, HI 96720, USA

Received 27 August 2007; received in revised form 6 November 2007; accepted 10 November 2007

Abstract

Remote sensing of invasive species is a critical component of conservation and management efforts, but reliable methods for the detection of invaders have not been widely established. In Hawaiian forests, we recently found that invasive trees often have hyperspectral signatures unique from that of native trees, but mapping based on spectral reflectance properties alone is confounded by issues of canopy senescence and mortality, intra- and inter-canopy gaps and shadowing, and terrain variability. We deployed a new hybrid airborne system combining the Carnegie Airborne Observatory (CAO) small-footprint light detection and ranging (LiDAR) system with the Airborne Visible and Infrared Imaging Spectrometer (AVIRIS) to map the three-dimensional spectral and structural properties of Hawaiian forests. The CAO-AVIRIS systems and data were fully integrated using in-flight and post-flight fusion techniques, facilitating an analysis of forest canopy properties to determine the presence and abundance of three highly invasive tree species in Hawaiian rainforests.

The LiDAR sub-system was used to model forest canopy height and top-of-canopy surfaces; these structural data allowed for automated masking of forest gaps, intra- and inter-canopy shadows, and minimum vegetation height in the AVIRIS images. The remaining sunlit canopy spectra were analyzed using spatially-constrained spectral mixture analysis. The results of the combined LiDAR-spectroscopic analysis highlighted the location and fractional abundance of each invasive tree species throughout the rainforest sites. Field validation studies demonstrated <6.8% and <18.6% error rates in the detection of invasive tree species at $\sim 7 \text{ m}^2$ and $\sim 2 \text{ m}^2$ minimum canopy cover thresholds. Our results show that full integration of imaging spectroscopy and LiDAR measurements provides enormous flexibility and analytical potential for studies of terrestrial ecosystems and the species contained within them.

© 2008 Elsevier Inc. All rights reserved.

Keywords: Airborne Visible and Infrared Imaging Spectrometer; AVIRIS; Carnegie Airborne Observatory; CAO; Hawaii; Invasive species; Light detection and ranging; Tropical forest

1. Introduction

Invasive species can alter the composition, structure, and functioning of terrestrial ecosystems. We consider a species invasive when it propagates across landscapes with or without facilitation by human or natural disturbance. Island ecosystems are particularly susceptible to biological invasion, owing to the

evolutionary effects of isolation that cause island flora to lack many of the competitive plant traits found in continental systems (Sax et al., 2002; Vitousek et al., 1997). Ecosystems of the Hawaiian Islands continue to undergo rapid changes following the introduction and proliferation of alien species (D'Antonio & Vitousek, 1992; Vitousek & Walker, 1989).

Roughly half of all organisms in Hawaii are non-native, and approximately 120 plant species are considered highly invasive (Wagner et al., 1999; www.hear.org). Highly invasive tree species demonstrate an ability to grow through the native canopy, or in

* Corresponding author. Tel.: +1 650 462 1047x200.

E-mail address: gpa@stanford.edu (G.P. Asner).

gaps, eventually replacing the native canopy (Vitousek & Walker, 1989; Yamashita et al., 2000). Invaders can alter fundamental ecosystem processes such as nitrogen (N) cycling (Ehrenfeld, 2003; Vitousek & Walker, 1989) and disturbance regimes (D'Antonio & Vitousek, 1992; Hughes et al., 1991). Recent work also shows that invasive tree species often express biochemical and physiological properties unique from those of native trees (Baruch & Goldstein, 1999; Funk & Vitousek, 2007; Hughes & Denslow, 2005). Resolving these particular leaf and canopy characteristics in remotely sensed imagery may provide a way to map and monitor invaders at the regional scale.

Robust approaches to mapping species are currently lacking because we have had a limited biophysical understanding of when remotely sensed signatures indicate the presence of unique species — native or invasive — within an ecosystem. Another major limitation has been the lack of appropriate technologies for isolating and analyzing the spectral properties of plant canopies. In Hawaii, we recently found that invasive tree species have unique spectroscopic reflectance signatures (or hyperspectral signatures) from that of native tree species (Asner et al., 2008-this issue). In that work, canopy reflectance properties in the 400–2500 nm wavelength range, collected from an improved version of the Airborne Visible and Infrared Imaging Spectrometer (AVIRIS; <http://aviris.jpl.nasa.gov>), demonstrated spectral separability of native, introduced and highly invasive species. Further analysis showed systematic, wavelength-dependent spectral reflectance differences between plant functional types, especially nitrogen-fixing and non-fixing trees. Most importantly, we showed that the spectral separability of species was tightly linked to their biochemical composition (Asner et al., 2008-this issue).

Although alien tree species in Hawaii often have unique spectroscopic reflectance properties linked to their biochemical traits, we were unable to use this information in a simple approach to map the species. Our initial study manually isolated sunlit portions of only the largest tree crowns in order to assess the spectral separability of species. However, application of this knowledge to AVIRIS and other imagery was confounded by issues of canopy senescence and mortality, intra- and inter-canopy gaps and shadowing, and terrain variability. Furthermore, we could not employ traditional multi-spectral methods that are often used to dampen shadowing and terrain effects, such as vegetation indices like the normalized difference vegetation index (NDVI), because the full spectral signature was required to separate species on a statistically robust basis (Asner et al., 2008-this issue).

An expanded approach that simultaneously resolves both the spectral and structural properties of the canopies is needed to isolate sunlit portions of tree crowns and to account for changes in underlying terrain. Whereas the spectral signatures can be derived from high-fidelity imaging spectrometers (Clark et al., 2005), the canopy structure and terrain data are often best resolved using Light Detection and Ranging (LiDAR) (Lefsky et al., 2002). However, the coordinated use of these two technologies, especially in the context of very detailed crown-by-crown mapping of species, requires highly precise co-location of the spectrometer and LiDAR data.

We have developed the Carnegie Airborne Observatory (CAO; <http://cao.stanford.edu>) to provide in-flight and post-flight fusion of imaging spectrometer and LiDAR data. We define data fusion as “the seamless integration of data from disparate sources, ... integrated across data collection platforms, ... and blended so that the differences in resolution and coverage, ... character and artifacts of data collection methods are eliminated” (<http://cee.uiuc.edu/people/kumar1/>). The CAO system is comprised of a small-footprint waveform LiDAR, an imaging spectrometer, a high-performance three-dimensional aircraft trajectory system, and new algorithms that ray trace the precise position of ground targets with respect to instruments on board the aircraft (Asner et al., 2007). Here we integrated AVIRIS as the spectrometer in the CAO system, allowing for a detailed integration of full-range (400–2500 nm) imaging spectroscopy and scanning LiDAR.

Using the CAO-AVIRIS system, we developed a method to detect the presence and extent of invasive tree species in five Hawaiian rainforest sites. Our automated approach uses the LiDAR data to quantify and mask sunlit tree crowns of a minimum prescribed height in the AVIRIS imagery, and then analyzes the hyperspectral properties of those pre-screened tree crowns using multi-stage spectral mixture analysis. A first spectral mixture analysis derives live and dead canopy fractional cover from shortwave-infrared (SWIR) measurements. A second mixture analysis estimates species-specific fractional canopy cover from the subset of original image pixels that pass the illumination, minimum height, and live:dead pre-screening. Our primary goal was to test the new method for mapping three highly invasive tree species in Hawaiian forests. A parallel goal was to continue testing the spectral separability of native and invasive tree species in Hawaii, as a means to advance our efforts to map and monitor their spread over time.

2. Materials and methods

2.1. Study sites

Our study was conducted in five rainforest sites spanning a precipitation range of 2000 to 4000 mm yr⁻¹ on the Island of Hawaii (Fig. 1; Table 1). The sites varied in size from 330 to 1395 ha, each chosen based on the accessibility of the forests on the ground as well as our general knowledge of species composition. All sites were once dominated by native Hawaiian forest species *Metrosideros polymorpha* and/or *Acacia koa*, with an understory mostly comprised of ferns *Cibotium glaucum* and *Dicranopteris linearis*.

Each study forest now contains a large, sprawling infestation of one or more highly invasive tree species (Table 1). *Fraxinus uhdei* was introduced in the late 19th century from Southern Mexico and Guatemala as a potential forest plantation species. It was later abandoned as a timber species due to poor wood properties, but continued to regenerate and proliferate on several islands including at a site in the Laupahoehoe Extension of the Hilo Forest Reserve, Hawaii (Fig. 1) (Carlson & Bryan, 1963; Francis, 1990). *Psidium cattleianum* was introduced to Hawaii in 1825 from Brazil, and is among the most highly invasive trees in the state (Smith, 1985). It is found extensively

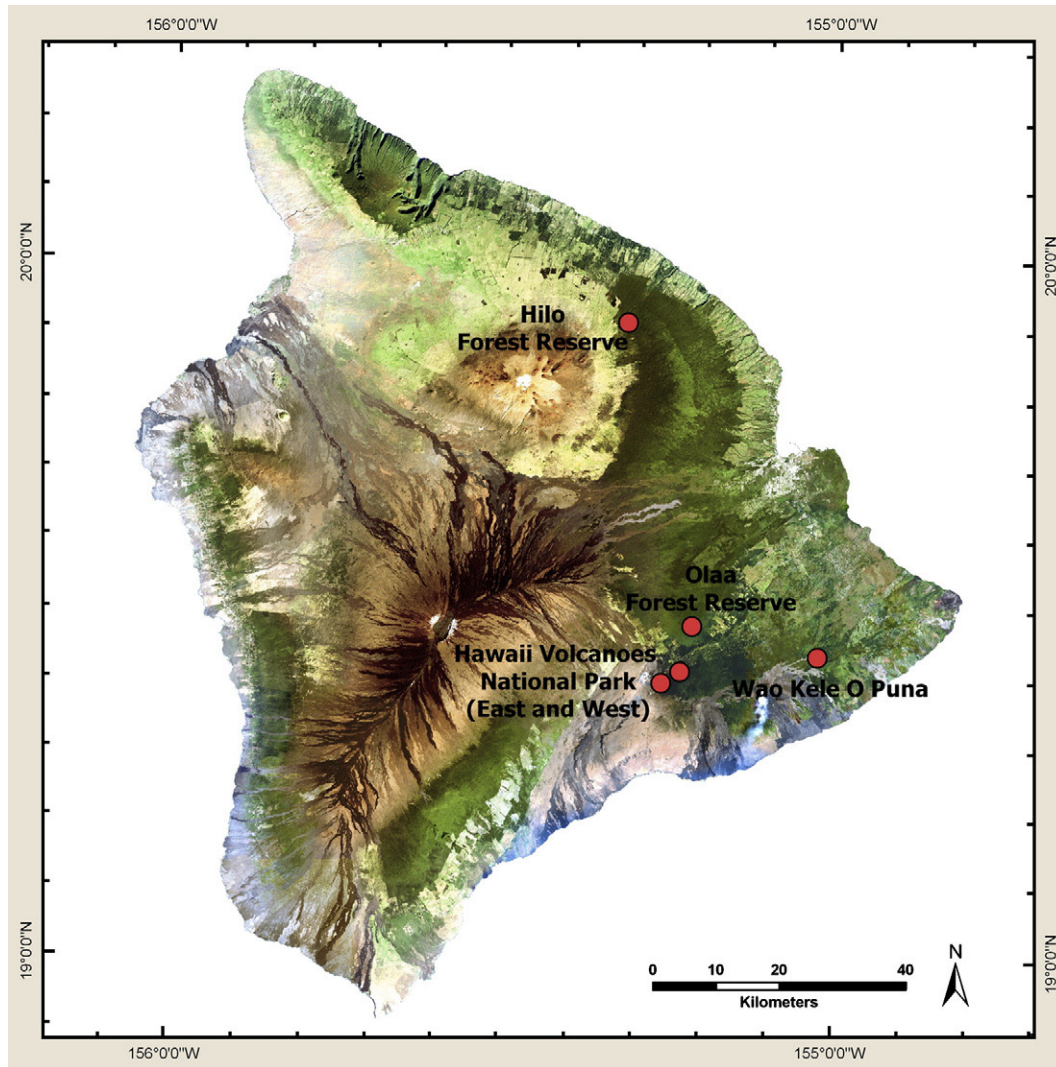


Fig. 1. The Island of Hawaii showing the central location of CAO-AVIRIS study areas (red dots).

in both mesic and wet forest areas, including two of our study sites: Olaa Forest Reserve and Wao Kele O Puna Natural Area Reserve. Finally, the nitrogen-fixing tree *Morella faya* (formerly *Myrica faya*) was introduced from the Azores to Hawaii Volcanoes National Park about fifty years ago (Fig. 1). It is also considered highly invasive, enriching the nitrogen content of otherwise low-fertility soils, while shading out nearly all other species (Vitousek et al., 1987). The three invasive species thus provided us with a diverse array of canopy chemistries and

structural properties for developing and testing our remote sensing approach.

2.2. Remote sensing instrumentation

Large-scale analysis of forest three-dimensional structure and biological composition requires a combination of advanced airborne imaging technologies that simultaneously resolves the horizontal and vertical characteristics of the vegetation as well

Table 1
Forest descriptions including site name, study area (ha), zone type, most common native and invasive canopy species, mean annual precipitation (MAP; mm yr⁻¹), mean annual temperature (MAT; °C), and substrate age (yr)

Site	Study area	Study zone	Common native	Common invasive	MAP	MAT	Substrate age
Hilo Forest Reserve	1395	Montane Rainforest	<i>M. polymorpha</i> & <i>A. koa</i>	<i>F. uhdei</i>	3000	17	5000–65,000
Wao Kele O Puna	620	Lowland Rainforest	<i>M. polymorpha</i>	<i>P. cattleianum</i>	3500	25	200–750
Olaa Forest Reserve	675	Sub-montane Rainforest	<i>M. polymorpha</i> & <i>A. koa</i>	<i>P. cattleianum</i>	4000	18	5000–10,000
Hawaii Volcanoes National Park–East	330	Montane Rainforest	<i>M. polymorpha</i>	<i>M. faya</i>	2500	20	300–400
Hawaii Volcanoes National Park–West	540	Seasonal Sub-montane Forest	<i>M. polymorpha</i>	<i>M. faya</i>	2000	22	100–300

as the type of vegetation, even to the species level. To address this need, we developed the Carnegie Airborne Observatory (CAO), a new system designed specifically for mapping the biochemical, taxonomic and structural properties of vegetation and ecosystems (<http://cao.stanford.edu>) (Asner et al., 2007). The CAO combines three instrument sub-systems into a single airborne package: (1) High-fidelity Imaging Spectrometer (HFIS); (2) Waveform Light Detection and Ranging (LiDAR) scanner; and (3) Global Positioning System-Inertial Measurement Unit (GPS-IMU).

There are two CAO configurations, depending upon the spectrometer used during flight. The CAO-Alpha configuration uses a pushbroom HFIS with 1500 cross-track pixels, and sampling across the 367–1056 nm range at up to 2.4 nm spectral resolution (Asner et al., 2007). The CAO-Beta system, which was employed in this study, integrates AVIRIS to provide 10 nm spectral sampling across the 380–2510 nm range. Both CAO

configurations use a LiDAR sub-system with an adjustable laser pulse repetition rate of up to 100 kHz. The GPS-IMU sub-system provides three-dimensional positioning and attitude data for the sensor package onboard the aircraft, allowing for highly precise and accurate projection of hyperspectral and LiDAR observations to the ground (Asner et al., 2007).

The CAO system provides co-aligned HFIS and LiDAR data at spatial resolutions of 0.3–3.5 m, depending on instrument settings on board the aircraft and flying altitude above ground. For this study, the CAO-Beta system was operated from January to February 2007 over Hawaii Island at an altitude averaging 3.0 km above ground level (a.g.l.), thus providing spectroscopic measurements at 3.0 m spatial resolution (ground sample distance). The LiDAR sub-system is programmable in-flight, and was configured here for laser spot spacing (postings) of 1.5 m. Due to the higher altitude requirements of AVIRIS, we operated the LiDAR at a pulse repetition frequency of 33 kHz and a scan

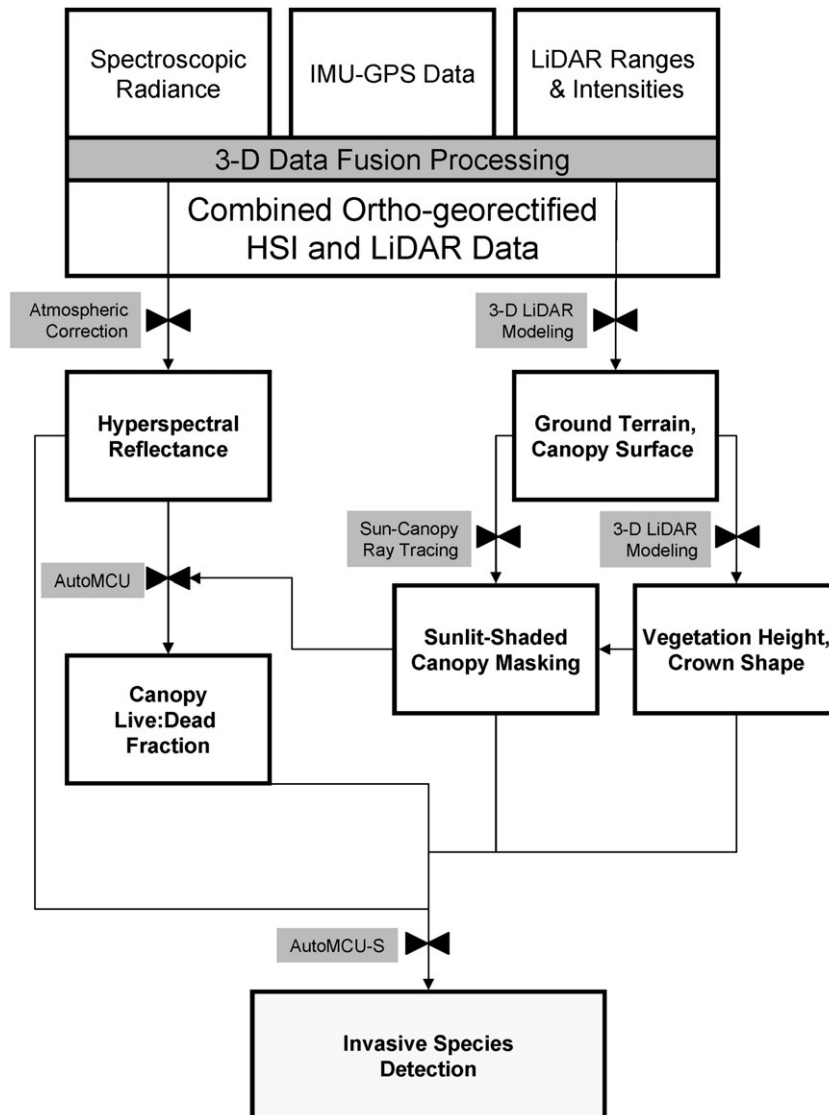


Fig. 2. The processing stream for in-flight and post-flight fusion of airborne imaging spectrometer and LiDAR observations, sunlit-live canopy detection, and invasive species mapping.

angle of 36° to match AVIRIS. The LiDAR thus collected four laser shots per spectrometer pixel, allowing for modeling of canopy structure and surface shape within each AVIRIS pixel.

2.3. Remote sensing data analysis

Fusion of the imaging spectrometer and LiDAR data requires a processing stream that maximizes the sharing of information between data products. Given the enormous data volumes involved, the processing stream must be highly automated. Fig. 2 shows the processing stream for this study, in which raw spectral, laser, and trajectory data were fused and analyzed in a series of higher-order products and results. The following sections briefly describe the major steps in the process.

2.3.1. Aircraft positioning

The CAO uses both in-flight and post-flight data fusion approaches to precisely match hyperspectral and LiDAR data in three-dimensional space. The in-flight fusion step was achieved by providing a common mount with measured offsets between instrument optical centers, as well as time-stamping of spectral and LiDAR data collection streams with shared position and trajectory data. The GPS-IMU data form the common link for the detailed ray tracing of the photons between both aircraft sensors and the ground, and a detailed model of the spectrometer optical system allows precise and accurate ray tracing of the image pixels to the LiDAR returns. The point-for-point alignment of the LiDAR and passive image data is complicated by inherent differences in the scanning geometries of the two systems and the further distortions of the ground sampling grid due to topography. The spectrometer pixel centers were used for rendering of the two data sets into a single, integrated grid of hyperspectral and LiDAR data for subsequent processing, analysis and product generation (Asner et al., 2007).

2.3.2. LiDAR data processing

The GPS-IMU data were combined with the laser range data to determine the 3-D location of the laser returns. From the LiDAR point cloud data, a physically-based model was used to estimate top-of-canopy and ground surfaces (digital elevation models; DEMs) using REALM (Optech Inc., Toronto, Canada) and Terrascan/Terramatch (Terrasolid Ltd., Jyväskylä, Finland) software packages. Vegetation height was then estimated by differencing the top-of-canopy and ground surface DEMs following (Clark et al., 2004; Lefsky et al., 2002, 1999).

2.3.3. Hyperspectral data processing

The hyperspectral data were converted to at-sensor radiances by applying radiometric corrections developed during sensor calibration in the laboratory. Apparent surface reflectance was then derived from the radiance data using an automated atmospheric correction model, ACORN 5LiBatch (ImSpec LLC, Palmdale, CA). Inputs to the atmospheric correction algorithm included ground elevation (from the LiDAR), aircraft altitude (from GPS-IMU), solar and viewing geometry, atmosphere type (e.g., tropical), and estimated visibility (in km). The code uses a MODTRAN look-up table to correct for Rayleigh

scattering and aerosol. Water vapor was estimated directly from the 940/1140 nm water vapor features in the radiance data.

Following the preparation of the hyperspectral data, the reflectance images were automatically masked based on illumination conditions between the sensors and canopies (Fig. 2). The LiDAR data, along with known solar position at time of data acquisition, provided three-dimensional maps of precise illumination geometry for each canopy element. If there were no obstructions in the sun-vegetation-sensor path (e.g., neighboring tree crowns, branches, stems), then that element was considered sunlit at the time of imaging. At the same time, a minimum LiDAR vegetation height requirement of 2.0 m was applied to remove exposed ground areas and short vegetation such as grasses and shrubs.

The masked hyperspectral images were passed to an automated spectral mixture analysis model called *AutoMCU* (Asner & Heidebrecht, 2002). This algorithm uses tied short-wave-infrared (tied-SWIR) (Asner & Lobell, 2000) spectra to quantify the fractional cover of photosynthetic vegetation (PV), non-photosynthetic vegetation (NPV), and bare substrate within each image pixel. The model uses spectral endmember bundles derived from field- or image-based measurements, and Monte Carlo unmixing to derive mean estimates of fractional cover along with standard deviation and root-mean-squared-error (RMSE) data on a per-pixel basis. The PV, NPV and bare-substrate spectral bundles were derived from island-wide samples collected using 2001–2005 AVIRIS imagery as well as field-based measurements with spectroradiometers (Asner et al., 2005). For our purposes here, only the NPV data derived from the *AutoMCU* were used to mask out the standing dead trees and other non-photosynthetic vegetation from the hyperspectral data (Fig. 2).

The image spectra that remained after illumination, shadow, vegetation height, and NPV masking represented a well controlled set of reflectance signatures that, theoretically, should be most indicative of unique species. The final automated step in the processing stream involved a new reformulated version of the *AutoMCU* algorithm to detect species using spectral bundles (Fig. 1). Whereas the previous step — running the *AutoMCU* in tied-SWIR spectral mode — isolated the fractional cover of live and dead vegetation with little influence from variation in taxonomic composition (Asner et al., 1999, 2005), application of *AutoMCU* with full-range spectral reflectance signatures (hereafter called “*AutoMCU-S*” mode) should be sensitive to the species that comprise the spectral bundles used in the model. A spectral unmixing approach was selected because crown diameters of native and invasive trees range from just a few meters to 30 or more meters; we thus required an algorithm that could accommodate a wide range of crown sizes and thus fractional cover values. *AutoMCU-S* uses the same Monte Carlo unmixing technique as the *AutoMCU*, but with species-specific endmember bundles to derive maps of fractional species cover per pixel, along with standard deviation and RMSE images.

In previous work, we collected image-based spectral bundles of 43 of the most common native and invasive tree species found in Hawaiian rainforests (Asner et al., 2008-this issue). Here, we applied the *AutoMCU-S* approach with a subset of

species bundles relevant to the region of interest. These were selected based on our general knowledge of the likely tree taxa to be present in each study forest. For example, a spectral bundle for *F. uhdei* was only used in the forests where this species is known to occur. This geographically-constrained use of the bundles simplified our detection and mapping problem, yet we felt it a necessary step in our effort to determine the maximum accuracy of the approach at the landscape scale. In addition, the general presence and absence of both native and invasive species is well known for most forests on Hawaii Island (Smith, 1985) (<http://www.hear.org>), so tuning the *AutoMCU-S* with regionally-specific libraries was justified from both scientific and land management perspectives.

For this study, we used 12 endmember bundles containing one native species collected from all five sites (*M. polymorpha*), one native species from two sites (*A. koa*), and three invasive species from all five sites (*M. faya*, *F. uhdei*, *P. cattleianum*). The libraries were constructed from spectra pre-screened for minimum height and illumination conditions using the co-aligned LiDAR data, and thus were compatible with the image data. Minimum height was set to 2.0 m, and only pixels containing canopies with unobstructed ray traces from the sun-

to-canopy and canopy-to-sensor were used in the library development and image analyses. In addition, only pixels with no detected NPV from the *AutoMCU* code were selected both for library construction and image processing.

The separability of the spectral bundles was analyzed using *t*-tests and cluster analysis. The *t*-tests were intended simply to highlight wavelength-specific differences between spectral bundles of native and invasive tree species. In contrast, the cluster analyses provided information on the separability of species-based on the entire spectrum as the signature, rather than as band-by-band comparisons. The spectral endmember bundles were analyzed using a hierarchical *k*-means cluster tree, with iterative clustering based on the Euclidean distance (Everitt, 1993). Pairwise Euclidean distance in *n*-dimensional space ($n=218$ AVIRIS bands) was calculated using the equation:

$$\sqrt{\sum |x_i - y_i|^2}$$

where x and y are the mean AVIRIS reflectance values at wavelength i . The *k*-means clustering approach iteratively moves spectra between clusters, minimizing variability within each cluster and maximizing variability between them. The Euclidean

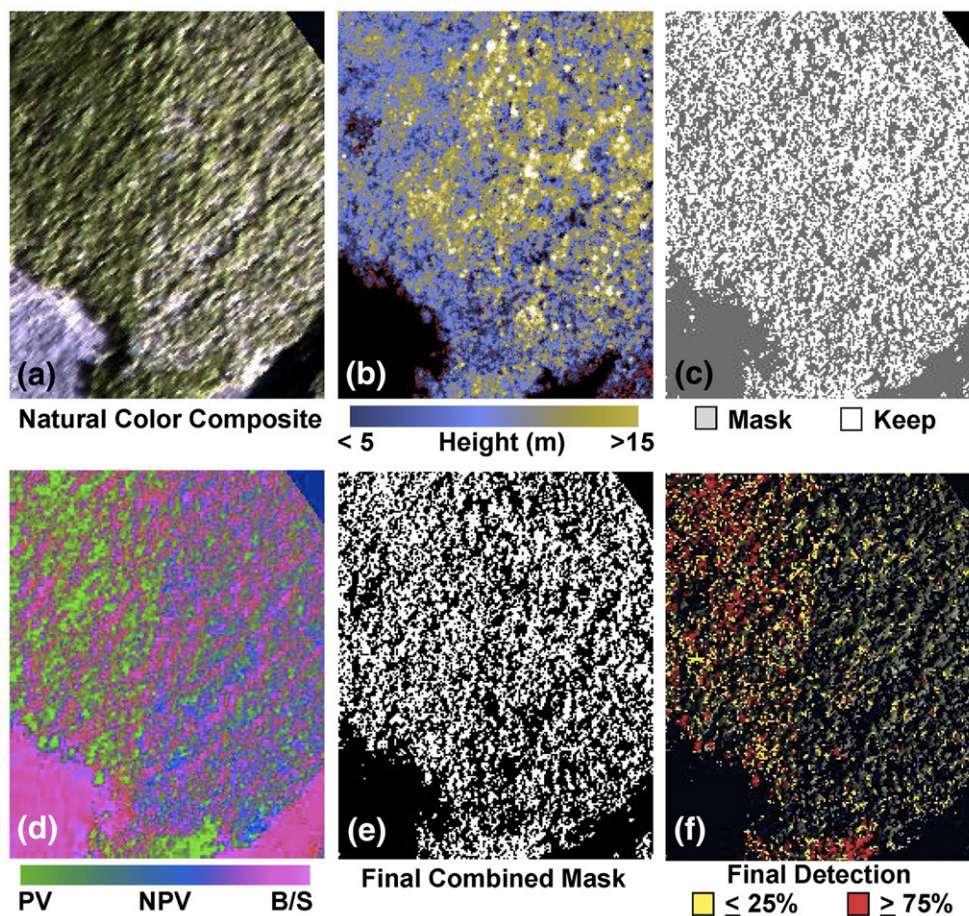


Fig. 3. Example output of each automated analysis step in the data fusion and invasive species detection process outlined in Fig. 2. This 53 ha example of the (a) basic reflectance imagery demonstrates the pre-screening of the spectrometer image data by (b) minimum vegetation height modeling from LiDAR data (ground: black; shorter canopies: red-dark blue; taller canopies yellow-white); (c) shadow masking based on 3-D structure of the canopies with respect to solar angle and sensor geometry (shadow: gray; sunlit: white); (d) live/dead fractional cover masking from *AutoMCU* modeling (PV: green; NPV: blue; bare/shade: pink); and (e) the final detection of an invasive tree based on spectral endmember bundles and *AutoMCU-S* algorithm (invader: yellow-red; native: green).

distance between clusters was tabulated as a measure of the spectral separability of species.

2.4. Field evaluation

We carried out field studies to evaluate the accuracy of our remote species detections in each forest stand. The analysis employed a combination of intensive plot-scale measurements, long field-based transect surveys, and low altitude helicopter surveys that identified false-positive and false-negative detections. The transects ranged from 200 m to 3000 m in length, with a total distance covered among sites of 16.3 km. Sampling was done according to Asner and Vitousek (2005) and Varga and Asner (in press), by which a point was recorded whenever the canopy cover changed, in this case, when the overstory changed in species dominance. Each change in species cover was recorded using a survey-grade GPS for co-location of field data with the airborne measurements. A Leica GS-50+GPS with multiple-bounce filtering and post-differential correction was used to measure our position in the forest to average uncertainties of ~ 2 m (Leica Geosystems Inc., St. Gallen, Switzerland). In addition, a ruggedized tablet computer with integrated GPS (Xplore Technologies, Austin, TX) was used to navigate in the forests, providing a real-time analysis and logging of our position with respect to the species identified in each digital map. Helicopter-based validation measurements were carried out by entering the coordinates of detected invasive species from the digital maps into a GPS with real-time Wide Area Augmentation System (WAAS) corrections (Thales Navigation, Santa Clara, CA). Each helicopter GPS point was visited from an altitude of <75 m a.g.l., with 2–3 observers determining canopy species cover. A total of 993 field and helicopter validation points were used in this study.

3. Results and discussion

3.1. Automated spectral masking

Fig. 3 shows the interim and final processing results for a sample 53 ha forest stand in Hawaii Volcanoes National Park containing the invasive tree *M. faya*. Here, the calibrated reflectance image (Fig. 3a) is aligned with the LiDAR vegetation height data (Fig. 3b), which along with known solar and sensor viewing geometries, allows for a deterministic mapping of sunlit and shaded tree crowns of a prescribed minimum 2.0 m height (Fig. 3c). This canopy illumination-minimum height mask is then re-combined with the reflectance spectra as input to the *AutoMCU* algorithm (Fig. 2), which calculates the sub-pixel fractional cover of PV, NPV and bare/shade (Fig. 3d). Any pixels with NPV values greater than zero are removed, since those pixels are influenced by standing dead trees and other senescent material that risk not carrying the spectral signature of the live species. This step results in a final determination of the spectra to be advanced to the species detection step, as shown in the final mask of Fig. 3e. Finally, the *AutoMCU-S* module provides sub-pixel fractional cover estimates of each species. This last panel shows *M. faya* detections at fractional cover values $>75\%$ in red and $>25\%$ in yellow, with native forest canopies shown in green. Pixels not meeting the pre-screening requirements for illumination conditions, minimum height or dead material are left unanalyzed, as shown in black in Fig. 3f.

The quantitative importance of masking pixels prior to species determination is shown in Fig. 4, which demonstrates how the mean and standard deviation of *M. faya* canopy reflectance changed before and after screening in Fig. 3. The unmasked spectral data of *M. faya* have a lower reflectance in the near-infrared and shortwave-infrared wavelength regions (750–1800 nm) than do the data following the masking step (Fig. 4).

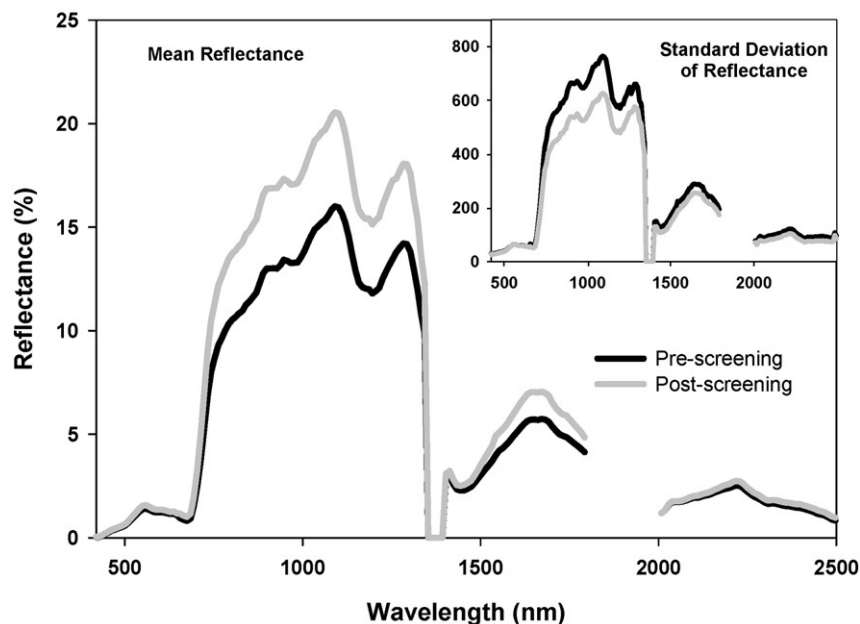


Fig. 4. Effect of pre-screening the spectra for minimum vegetation height, illumination conditions, and live:dead fraction on the mean and standard deviation (inset) of reflectance for the invasive tree *M. faya*. Number of samples prior to screening was >400 , whereas the number is decreased to 210 following all masking steps.

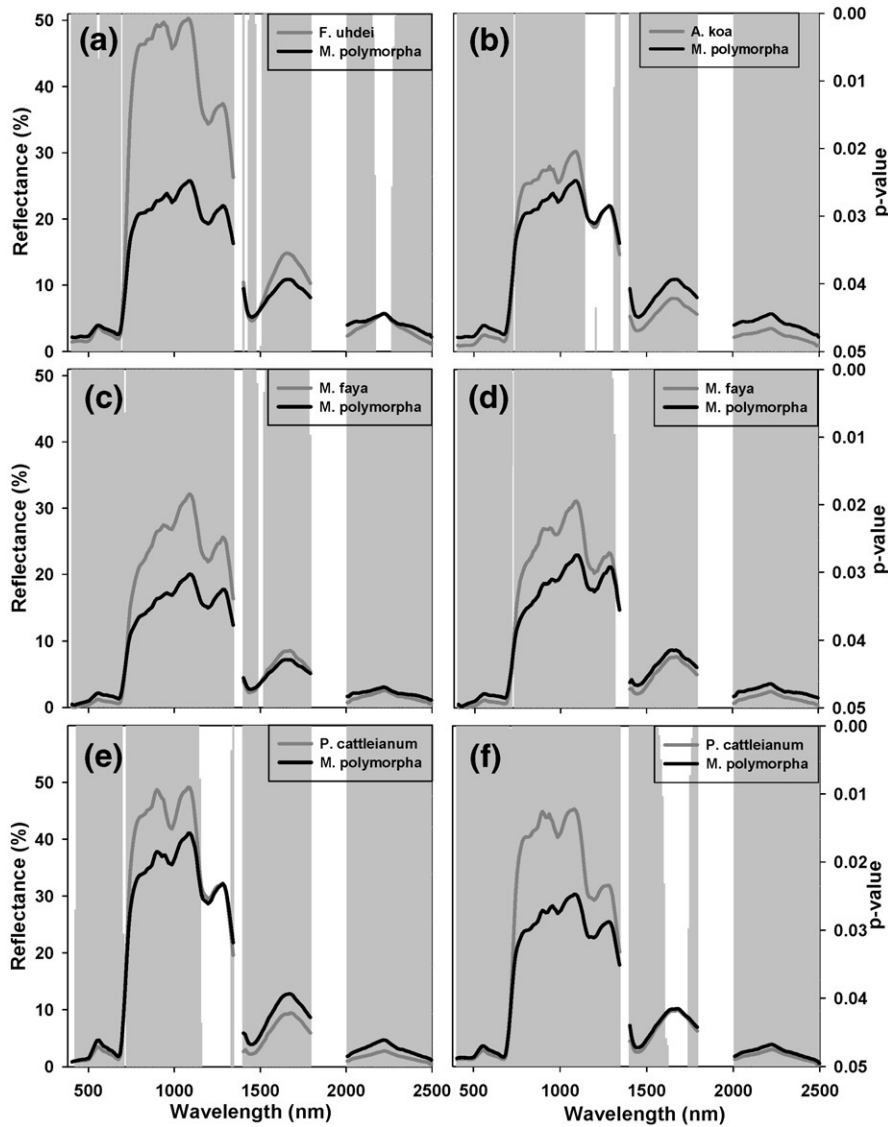


Fig. 5. Mean reflectance spectra of native and invasive tree detections following pre-screening (Fig. 3), with band-by-band *t*-tests showing significant differences in grey bars (p -values ≤ 0.05 ; $n=210$ – 239 as shown in Table 2). Sites: (a–b) Hilo Forest Reserve; (c–d) Hawaii Volcanoes National Park east–west; (e) Olaa Forest Reserve; and (f) Wao Kele O Puna Natural Area Reserve.

At the same time, the standard deviation of *M. faya* reflectance is much higher prior to screening and masking, especially in the near-IR. Following masking, the reflectance of this invader is

much higher and its variability decreases, resulting in a species-specific endmember bundle that is statistically more unique from that of native species (Fig. 5). Tests with this image, and 26 field

Table 2
Minimum Euclidean distances between species-based spectral endmember bundles derived from *k*-means clustering algorithm

Site	Species combination	Cluster distance after masking	Number of spectra
Hilo Forest Reserve	<i>M. polymorpha</i> / <i>F. uhdei</i> *	171.6	210/210
	<i>A. koa</i> / <i>F. uhdei</i> *	155.7	220/210
	<i>M. polymorpha</i> / <i>A. koa</i>	61.3	210/220
Wao Kele O Puna	<i>M. polymorpha</i> / <i>P. cattleanum</i> *	108.5	220/220
	<i>M. polymorpha</i> / <i>P. cattleanum</i> *	105.4	220/220
	<i>A. koa</i> / <i>P. cattleanum</i> *	119.3	239/220
Olaa Forest Reserve	<i>M. polymorpha</i> / <i>A. koa</i>	108.1	220/239
	<i>M. polymorpha</i> / <i>M. faya</i> *	82.3	210/210
Hawaii Volcanoes National Park–East	<i>M. polymorpha</i> / <i>M. faya</i> *	88.6	210/210

Distance values indicate the uniqueness of species bundles, with high separability shown as values exceed 50.0 (Everitt, 1993). Asterisks (*) denote invasive tree species.

validation points, showed that minimizing the spectral variance within a target species using the hyperspectral-LiDAR screening steps described above resulted in an increase in mapping accuracy from 63% to 91%. This serves as a general estimate of the positive effect in using the data fusion method presented here.

Fig. 5 shows the mean reflectance of the final species bundles for each forest study site. The gray bars display the significances (p -value) of differences between species calculated from simple band-by-band t -tests. Similar to the results from (Asner et al., 2008-this issue), we find that native and invasive species are highly separable in most wavelength regions. These spectral differences result from the fact that leaf nitrogen concentrations are systematically higher in invasive tree species as compared to native trees in Hawaiian forests (Baruch &

Goldstein, 1999; Funk & Vitousek, 2007; Vitousek & Walker, 1989). In addition, the leaf area index (LAI) and total canopy water content were found to be higher among many invasive tree species (Asner & Vitousek, 2005). Most importantly, a combination of leaf nitrogen, pigments, and canopy structural properties has proven consistently different between invasive and native trees in Hawaii (Asner et al., 2008-this issue).

These spectral differences among native and invasive tree species facilitate mapping and monitoring efforts in Hawaii, but only after the spectral images and the extracted endmember bundles are screened for illumination, minimum height, and NPV fraction to eliminate excessive variability. Using the k -means cluster analysis, we calculated the statistical distance between spectral endmember bundles after masking (Table 2).

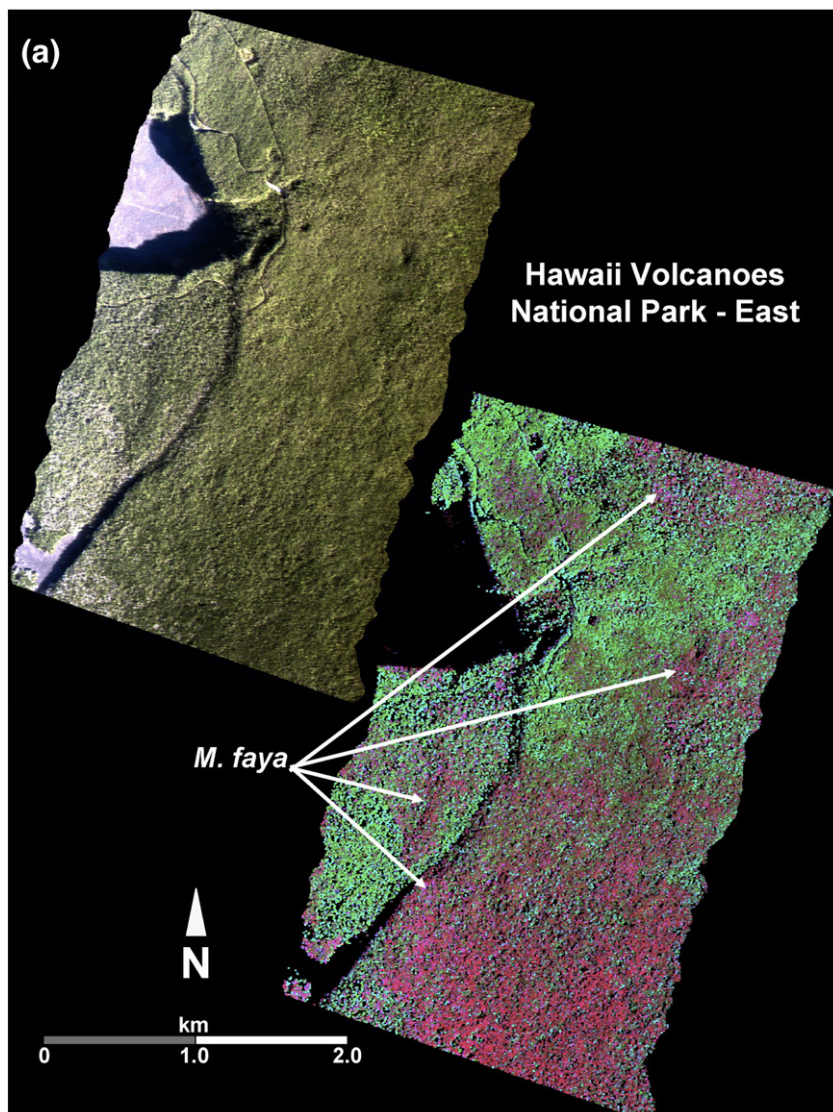


Fig. 6. a. Mapping results of constrained *AutoMCU-S* analysis for the detection of invasive *M. faya* trees (red colors) and native *M. polymorpha* trees (green colors) in Hawaii Volcanoes National Park—East. Fig. 6b. Top panel: Mapping results of constrained *AutoMCU-S* analysis for the detection of invasive *M. faya* trees (reds) and native *M. polymorpha* trees (greens) in Hawaii Volcanoes National Park—West. Bottom panel: Invasive *F. uhdei* (orange), native *A. koa* (yellow-green) and native *M. polymorpha* (blue-purple) in Hilo Forest Reserve. Fig. 6c. Top panel: Mapping results of constrained *AutoMCU-S* analysis for the detection of invasive *P. cattleanum* trees (reds), native *A. koa* (green) and native *M. polymorpha* (blue) in Olaa Forest Reserve. Bottom panel: Invasive *P. cattleanum* trees (reds) and native *M. polymorpha* (green) in Wao Kele O Puna Natural Area Reserve.

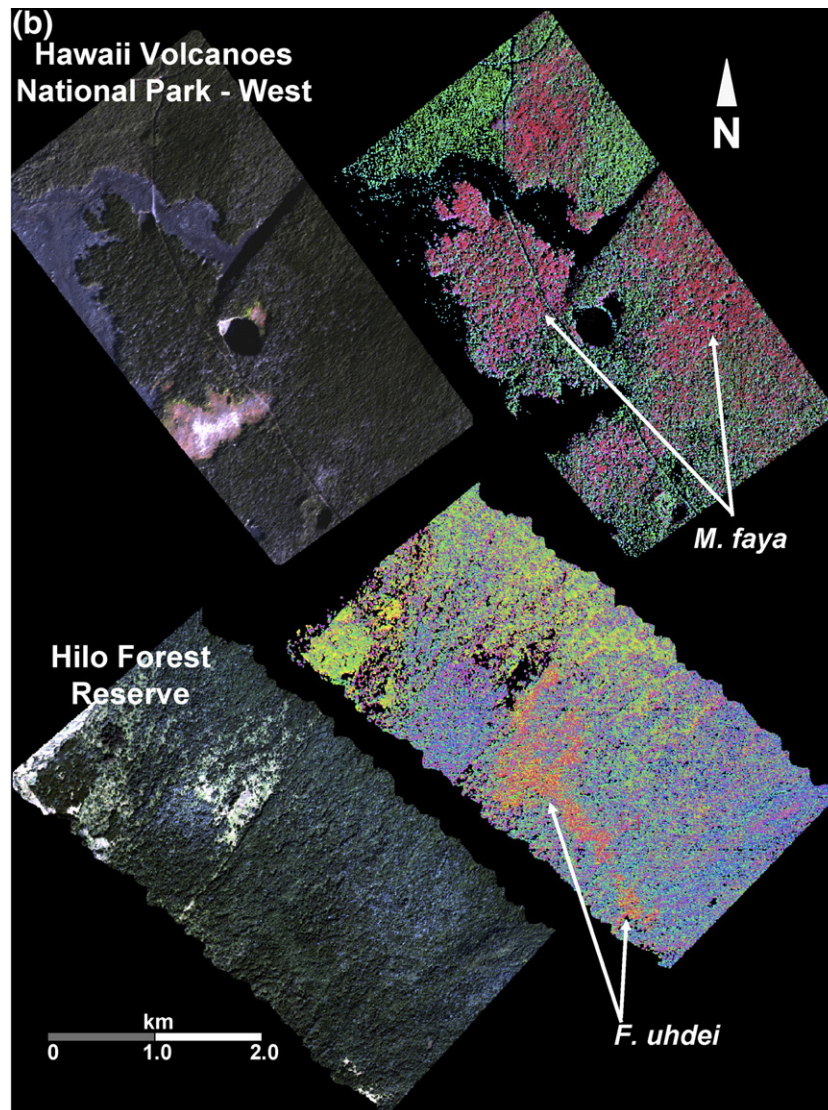


Fig. 6 (continued).

Cluster distances among native and invasive trees are large, ranging from about 82–172 units, which indicates excellent statistical separability (Everitt, 1993). In contrast, cluster distances between two groups of the native *M. polymorpha* taken from different forests average 31–64 (data not shown), which suggests some spectral differences between native forest systems dominated by this species, as documented by Asner et al. (2008-this issue). Promisingly, spectral differences between the native nitrogen-fixer *A. koa* and non-fixing natives such as *M. polymorpha* range from 61 to a maximum of 108 (Table 2), suggesting good spectral separability among native trees from contrasting functional groups. Without the screening steps afforded by the fused LiDAR and spectrometer data, the spectral bundles are far more variable and are difficult to interpret at the species level. Masking provides a much clearer delineation of species for a variety of methods, including the new automated Monte Carlo unmixing for species (AutoMCU-S) as reported in the next section.

3.2. Invasive species detection

The final invasive species maps are shown in Fig. 6a–c. The overall fidelity of the detection results is demonstrated in the *M. faya* map of Hawaii Volcanoes National Park–East (Fig. 6a). The natural color composite map hints of the presence of a differing vegetation type (dark greens), yet the processed data emphasize the location and abundance of *M. faya*, shown as increasing intensities of red as *M. faya* fractional cover increases at 3 m spatial resolution. Small outbreaks of this invader are also shown, sometimes at low fractional cover (darker reds), indicating the presence of newly established plants, usually in the sapling to small-tree phase (field observations, R. Martin and K. Carlson). In this forest, we detected 145.2 ha of total canopy cover by *M. faya*, which represented 44.0% of the total image, and 63.4% of the pixel analyzed following masking (Table 3). The majority of the infestations maintained sub-pixel fractional covers of <50%

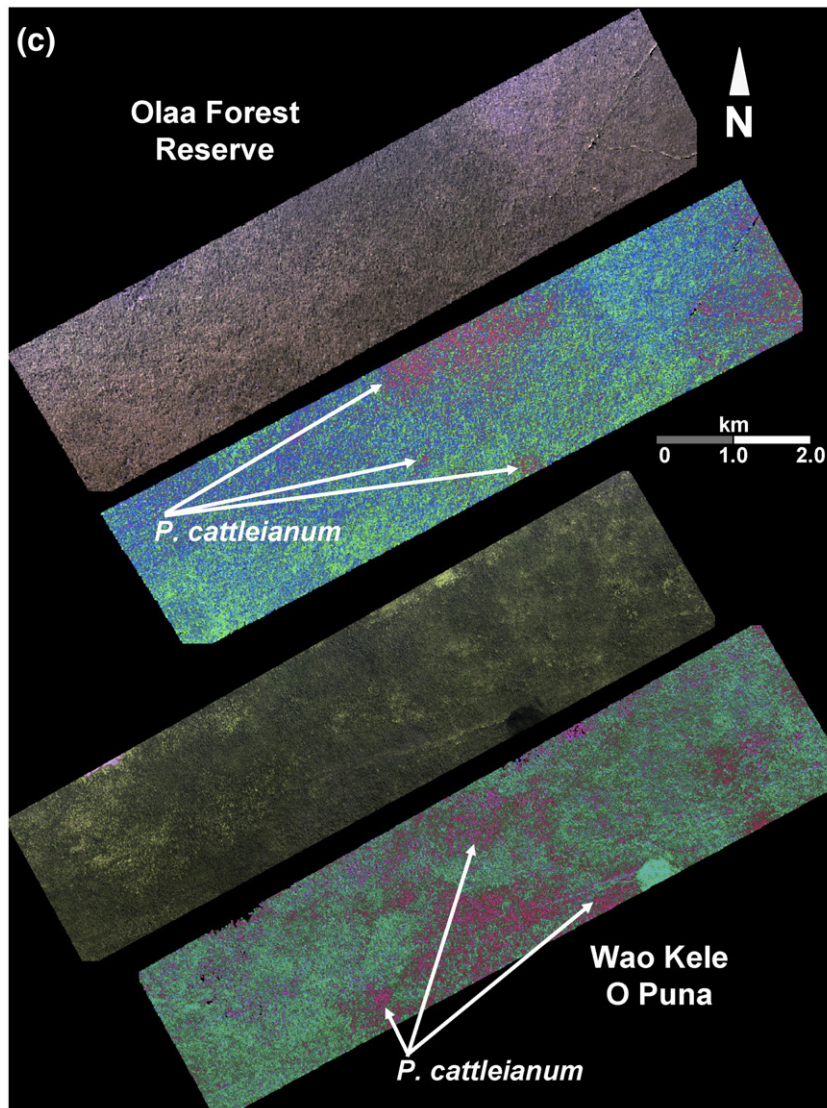


Fig. 6 (continued).

(61.9 ha), while 34.2 ha of cumulative detections had fraction canopy covers exceeding 75% per pixel.

M. faya was also detected in dense patches and outbreaks in the Hawaii Volcanoes National Park-West study area (top of Fig. 6b). We calculated 93.8 ha, or 17.4%, of the total study area was invaded by this species. Similar to the eastern study site, most canopy cover fractions were less than 50% per pixel (62.9 ha cumulatively), but fewer patches were completely covered by *M. faya* (8.6 ha with >75% fractional cover) (Table 3).

In Hilo Forest Reserve, *F. uhdei* was detected in 71.3 ha of the 1395 ha study area (Fig. 6b). Although this species is contained within a relatively contiguous forest patch, we did detect numerous small outbreaks, found later to be single tree crowns up to 600 m from the core area of infestation (oranges in Fig. 6b). Most of the *F. uhdei* trees covered <75% of any given pixel (66.9 ha cumulatively), even within the core area, with just 4.4 ha of canopy totally dominated by *F. uhdei* in the sub-pixel fractional cover results (Table 3).

The third major invasive tree species in Hawaii, *P. cattleianum*, was also readily detected in the Olaa and Wao Kele O Puna reserves, as shown in Fig. 6c. Similar to the *F. uhdei* results, the infestation of *P. cattleianum* within Olaa Forest Reserve was formed in a core area, with outbreaks detected up to 1.5 km from this core (red in top of Fig. 6c). A total of 110.5 ha of this species were mapped, which represented 16.4% of the total study area (Table 3). The majority of detections had sub-pixel cover fractions <75% (100.9 ha total). In contrast to Olaa, the *P. cattleianum* invasions in Wao Kele O Puna was more diffuse, with several infestation nuclei and many patches representing outbreaks of this invader (red in bottom of Fig. 6c). The core areas were comprised of *P. cattleianum* at fractional covers well over 75% per pixel, and these areas summed to 24.8 ha of the total 139.8 ha of detections (Table 3). However, the majority of patches (100.8 ha in total) contained outbreaks with fractional cover values less than 50%, indicating these areas as relatively new invasions within this rainforest reserve.

Table 3

Summary results for invasive species mapping including overall study area, analysis area following masking, area invaded (ha) by fractional cover class from *AutoMCU-S*, total area of invasion, and percent of analysis and total study areas invaded

Site	Total study area (ha)	Analysis area (ha)	Area invaded by fractional cover class	Total invaded area (ha)	% of analysis area	% of total study area
Hilo Forest Reserve	1395	799	<50%: 35.8 50–75%: 31.1 >75%: 4.4	71.3	8.9	5.1
Wao Kele O Puna	620	588	<50%: 100.8 50–75%: 14.2 >75%: 24.8	139.8	23.8	22.5
Olaa Forest Reserve	675	542	<50%: 43.1 50–75%: 57.8 >75%: 9.6	110.5	20.4	16.4
Hawaii Volcanoes National Park–East	330	229	<50%: 61.9 50–75%: 48.9 >75%: 34.2	145.2	63.4	44.0
Hawaii Volcanoes National Park–West	540	112	<50%: 62.9 50–75%: 22.3 >75%: 8.6	93.8	83.8	17.4

3.3. Field evaluation

We tabulated invasive species detections at *AutoMCU-S* thresholds of >25% (~2 m²) and >75% (~7 m²) fractional cover, and compared those results to the field- and helicopter-based validation points (Table 4). In Hilo Forest Reserve, we visited 164 points in the field, and calculated a 1.0% false-negative and 15.5% false-positive error rate for *F. uhdei* when

Table 4
Validation results for invasive species detection

Hilo Forest Reserve	<i>F. uhdei</i> (n=164)	Observed	Observed	Percentage error
		No	Yes	
Detected	No	92/93	1/0	1.0/0.0
Detected	Yes	11/3	60/68	15.5/4.2
Wao Kele O Puna	<i>P. cattleianum</i> (n=64)	Observed	Observed	
		No	Yes	
Detected	No	31/34	3/1	8.5/2.8
Detected	Yes	3/0	26/29	10.5/0.0
Olaa Forest Reserve	<i>P. cattleianum</i> (n=141)	Observed	Observed	
		No	Yes	
Detected	No	96/109	22/8	18.6/6.8
Detected	Yes	2/0	21/23	8.6/0.0
Hawaii Volcanoes–East	<i>M. faya</i> (n=405)	Observed	Observed	
		No	Yes	
Detected	No	166/180	20/6	10.8/3.2
Detected	Yes	31/9	188/211	14.2/4.1
Hawaii Volcanoes–West	<i>M. faya</i> (n=256)	Observed	Observed	
		No	Yes	
Detected	No	118/130	16/4	11.9/3.0
Detected	Yes	11/6	111/116	9.0/4.9

Values separated by slash (/) indicates detection results at 25% (~2 m²) and 75% (~7 m²) fractional cover levels from *AutoMCU-S* output for each species.

the *AutoMCU-S* cover threshold was 25% for that species. Increasing to a 75% minimum cover requirement decreased the errors to 0% and 4% for false-negative and -positive detections, respectively. For the invasive tree *P. cattleianum* in the Wao Kele O Puna and Olaa forest sites, the 25% and 75% detection thresholds produced false-negative errors ranging from 8.5–18.6% and 2.8–6.8%, respectively (Table 4). False-positive errors varied from 8.6–10.5% at the lower detection threshold, but were zero at the higher threshold for both forest sites. *M. faya* was detected throughout Hawaii Volcanoes National Park with false-negative errors of 10.8–11.9% and 3.0–3.2% at the 25% and 75% minimum fractional cover thresholds. False-positive errors were 9.0–14.2% and 4.1–4.9% at these two thresholds.

These low error rates are linked to the strong spectral separability of the species (Table 2), which results from the unique properties of invasive and native trees found in most Hawaiian forests. Specifically, a combination of high leaf nitrogen, differences in leaf pigments, and contrasting leaf area index (LAI) and canopy water content makes the three invasive tree species studied here, as well as many others (Asner et al., 2008-this issue), spectrally unique from most of their native Hawaiian neighbors. The particularly low uncertainties in the *F. uhdei* results are clearly connected to the large statistical distances between spectral clusters of this species relative to the native species *M. polymorpha* and *A. koa* (Table 2). The other invasive trees, *P. cattleianum* and *M. faya*, had smaller clustering distances to their native counterparts, resulting in slightly elevated levels of uncertainty in their detection at the lower fractional cover threshold of 25%.

4. Conclusions

Remote sensing is beginning to play a more active role in efforts to detect, monitor and manage invasive species. Broadband multi-spectral methods have been successfully used to map invasive species that represent unique lifeforms in the communities they invade; a good example is shrub invasion into grasslands, and grass

invasion into shrublands (Lass, 2005). Habitat suitability analyses are also being carried out using spaceborne multi-spectral imaging (Morissette et al., 2006), allowing managers to consider future areas of potential invasion.

In contrast to these successes, the detection of species of similar lifeform has proven more difficult, requiring more data such as from hyperspectral sensors and often complicated analytical techniques. Underwood et al. (2006) used hyperspectral data with classification methods to map invasive aquatic plants in central California wetlands. Asner and Vitousek (2005) used airborne imaging spectroscopy and radiative transfer modeling to detect the nitrogen-fixing tree *M. faya* in a Hawaiian forest. That study also highlighted the difficulty of detecting smaller patches and sub-pixel cover fractions of *M. faya* in the forest. A subsequent bottom-up analysis of the spectral separability of trees in Hawaii showed that this invasive tree species, and many others, are systematically unique from most native species (Asner et al., 2008-this issue). However, that study enjoyed the luxury of hand-picking spectral signatures from only the largest tree crowns and under constant illumination conditions. Further analyses showed that shadows, terrain, and non-photosynthetic vegetation caused great uncertainty in any top-down mapping efforts.

In response to these substantial limitations, and the continuing need for more robust invasive species maps for conservation and management of Hawaiian forests (<http://www.hear.org>), we deployed a new hybrid airborne remote sensing system combining LiDAR and imaging spectroscopy to map the three-dimensional spectral and structural properties of Hawaiian forests. The spectral and LiDAR data were fully integrated using new in-flight and post-flight fusion techniques, facilitating an analysis of forest canopy properties that best determine the presence and abundance of invasive tree species in Hawaiian rainforests.

In this first study, we limited our approach by using spectral endmember bundles derived from canopies of known species within each image. This approach worked well, allowing for the mapping of each invasive tree with relatively high accuracy. Indeed, our field evaluation studies showed <6.8% and <18.6% error rates in the detection of invasive tree species at $\sim 7 \text{ m}^2$ and $\sim 2 \text{ m}^2$ canopy cover thresholds in a very densely populated rainforest environment. However, the next test of the approach will involve combining species-specific bundles for application across an ensemble of hyperspectral images containing many more native and invasive trees. Until then, our current results show that the integration of imaging spectroscopy and LiDAR remote sensing sensors and measurements provide enormous flexibility and analytical potential for studies of invasive species and biodiversity in tropical forest ecosystems.

Acknowledgements

We thank M. Eastwood, C. Sarture, S. Lundeen, P. Gardner, R. Green, and the Jet Propulsion Laboratory for the spirited effort to integrate AVIRIS into the Carnegie Airborne Observatory. We thank D. Muchoney and three anonymous reviewers for their helpful comments on the manuscript. Access

to field sites was provided by the U.S. National Park Service and the State of Hawaii Division of Forestry and Wildlife. This work was supported by NASA Terrestrial Ecology and Biodiversity Program grant NNG-06-GI-87G and the Carnegie Institution. The Carnegie Airborne Observatory is supported by the W.M. Keck Foundation and William Hearst III.

References

- Asner, G. P., Bateson, C. A., Wessman, C. A., & Privette, J. L. (1999). Impact of tissue, canopy and landscape properties on the reflectance of arid ecosystems. *Remote Sensing of Environment*, *74*, 69–84.
- Asner, G. P., Elmore, A. J., Hughes, F. R., & Vitousek, P. M. (2005). Ecosystem structure along bioclimatic gradients in Hawai'i from imaging spectroscopy. *Remote Sensing of Environment*, *96*, 497–508.
- Asner, G. P., & Heidebrecht, K. B. (2002). Spectral unmixing of vegetation, soil and dry carbon cover in arid regions: comparing multispectral and hyperspectral observations. *International Journal of Remote Sensing*, *23*, 3939–3958.
- Asner, G. P., Jones, M. O., Martin, R. E., Knapp, D. E., & Hughes, R. F., 2008. Remote sensing of native and invasive species in Hawaiian forests. *Remote Sensing of Environment*, *112*, 1912–1926 (this issue). doi:10.1016/j.rse.2007.02.043
- Asner, G. P., Knapp, D. E., Kennedy-Bowdoin, T., Jones, M. O., Martin, R. E., Boardman, J., et al. (2007). Carnegie Airborne Observatory: In-flight fusion of hyperspectral imaging and Light Detection and Ranging (LiDAR) for three-dimensional studies of ecosystems. *Journal of Applied Remote Sensing*. doi:10.1117/12.779590
- Asner, G. P., & Lobell, D. B. (2000). A biogeophysical approach for automated SWIR unmixing of soils and vegetation. *Remote Sensing of Environment*, *74*, 99–112.
- Asner, G. P., & Vitousek, P. M. (2005). Remote analysis of biological invasion and biogeochemical change. *Proceedings of the National Academy of Sciences*, *102*, 4383–4386.
- Baruch, Z., & Goldstein, G. (1999). Leaf construction cost, nutrient concentration, and net CO₂ assimilation of native and invasive species in Hawaii. *Oecologia*, *121*, 183–192.
- Carlson, N. K., & Bryan, L. W. (1963). The Honaunau Forest: An appraisal after seven years of planting. *Journal of Forestry*, *61*, 643–647.
- Clark, M. L., Clark, D. B., & Roberts, D. A. (2004). Small-footprint Lidar estimation of sub-canopy elevation and tree height in a tropical rain forest landscape. *Remote Sensing of Environment*, *91*, 68–89.
- Clark, M. L., Roberts, D. A., & Clark, D. B. (2005). Hyperspectral discrimination of tropical rain forest tree species at leaf to crown scales. *Remote Sensing of Environment*, *96*, 375–398.
- D'Antonio, C. M., & Vitousek, P. M. (1992). Biological invasions by exotic grasses, the grass/fire cycle, and global change. *Annual Review of Ecology and Systematics*, *23*, 63–87.
- Ehrenfeld, J. G. (2003). Effects of exotic plant invasions on soil nutrient cycling processes. *Ecosystems*, *6*, 503–523.
- Everitt, B. S. (1993). *Cluster analysis*. New York: Halsted Press.
- Francis, J.K. (1990). *Fraxinus uhdei* (Wenzig) Lingelsh. In: USDA Forest Service Technical Report SO-ITF-SM-28.
- Funk, J. L., & Vitousek, P. M. (2007). Resource-use efficiency and plant invasion in low-resource systems. *Nature*, *446*, 1079–1081.
- Hughes, F. R., & Denslow, J. S. (2005). Invasion by a N₂-fixing tree alters function and structure in wet lowland forests of Hawaii. *Ecological Applications*, *15*, 1615–1628.
- Hughes, R. F., Vitousek, P. M., & Tunison, T. (1991). Alien grass invasion and fire in the seasonal submontane zone of Hawai'i. *Ecology*, *72*, 743–746.
- Lass, L. W. (2005). A review of remote sensing of invasive weeds and example of the early detection of spotted knapweed and babysbreath with a hyperspectral sensor. *Weed Science*, *53*, 242–251.
- Lefsky, M. A., Cohen, W. B., Parker, G. G., & Harding, D. J. (2002). Lidar remote sensing for ecosystem studies. *BioScience*, *52*, 19–30.
- Lefsky, M. A., Harding, D., Cohen, W. B., Parker, G., & Shugart, H. H. (1999). Surface lidar remote sensing of basal area and biomass in deciduous forests of eastern Maryland, USA. *Remote Sensing of Environment*, *67*, 83–98.

- Morisette, J. T., Jarnevich, C. S., Ullah, A., Cai, W., Pedelty, J. A., Gentle, J. E., et al. (2006). A tamarisk habitat suitability map for the continental United States. *Frontiers in Ecology and Environment*, 4, 11–17.
- Sax, D. F., Gaines, S. D., & Brown, J. H. (2002). Species invasions exceed extinctions on islands worldwide: A comparative study of plants and birds. *The American Naturalist*, 160, 766–783.
- Smith, C. W. (1985). Impact of alien plants on Hawai'i's native biota. In C. P. Stone & J. M. Scott (Eds.), *Hawai'i's terrestrial ecosystems: Preservation and management* (pp. 180–250). Honolulu, Hawaii: University of Hawaii Cooperative National Park Resources Studies Unit.
- Underwood, E. C., Mulitsch, M. J., Greenberg, J. A., Whiting, M. L., Ustin, S. L., & Kefauver, S. C. (2006). Mapping invasive aquatic vegetation in the Sacramento–San Joaquin Delta using hyperspectral imagery. *Environmental Monitoring and Assessment*, 12, 47–64.
- Varga, T. A., & Asner, G. P. (in press). Hyperspectral and LiDAR remote sensing of fire fuels in Hawaii Volcanoes National Park. *Ecological Applications*.
- Vitousek, P. M., D'Antonio, C. M., Loope, L. L., Rejmanek, M., & Westbrooks, R. (1997). Introduced species: A significant component of human-caused global change. *New Zealand Journal of Ecology*, 21, 1–16.
- Vitousek, P. M., & Walker, L. R. (1989). Biological invasion by *Myrica faya* in Hawai'i: Plant demography, nitrogen fixation, ecosystem effects. *Ecological Monographs*, 59, 247–265.
- Vitousek, P. M., Walker, L. R., Whiteacre, L. D., Mueller-Dombois, D., & Matson, P. A. (1987). Biological invasion by *Myrica faya* alters ecosystem development in Hawaii. *Science*, 238, 802–804.
- Wagner, W.L., Herbst, D.R., & Sohmer, S.H. (1999). *Manual of the Flowering Plants of Hawai'i*. Honolulu: University of Hawaii Press and Bishop Museum Press.
- Yamashita, N., Ishida, A., Kushima, H., & Tanaka, N. (2000). Acclimation to sudden increase in light favoring an invasive over native trees in subtropical islands, Japan. *Oecologia*, 125, 412–419.